Exploring Dynamically Controlled Frisbee Throws Using a Highly Compliant Robotic Arm

Kai Junge[1] and Josie Hughes[1]

***Abstract*— When humans perform dynamic motions such as throwing, the passive properties such as the stiffness and damping of their arm is known to contribute to the task performance. By developing a robot arm which enables the stiffness of the different joints to be set programmatically, its contribution to the throwing behaviours can be determined. In addition to enabling new capabilities in robots this can also be useful for understanding how humans may perform such tasks. Utilizing permanent magnet synchronous motors (PMSM) and integrating them in back-drivable configurations we present a method of achieving programmable, precise, high bandwidth stiffness control. With a two joint variable stiffness arm, we experimentally explore the role of stiffness and coordination of actuation timings for the throwing of a Frisbee disk. From this exploration key trends between stiffness and the throwing distance and angle are observed. Considering variable stiffness (VS) we also see that the role and significance of VS varies depending on the overall energy levels of the system. For low energies, having a constant torque profile can enable a 30% increase in throwing distance, where as at higher energies VS is less significant. When compared to human throwers, the robot performs comparable to experienced humans for a short distance throwing task.**

I. Introduction

Humans and animals have a remarkable ability to execute a variety of different complex dynamical tasks, which often exploits their physical structure and form, and their ability to dynamically vary their compliance. Variable stiffness has been shown to have a significant role on locomotion [1] and explosive motion tasks [2]. The role of compliance (or more generally the variation of forces), and coordination of muscles can be hard to characterize. To enable robots to perform dynamic tasks with human levels of competency, the control of its compliance must be explored, understood, and optimized [3]. This also could bring about insights into mechanisms by which humans exploit stiffness and variable compliance. With an increased focus on soft and compliant robotic systems [4], developing technologies that enable compliant behaviour is timely and fundamental to exploring how this contributes to dynamic task capabilities [5].

We chose to focus and explore the task of Frisbee throwing using a robot arm that mimics the forearm and wrist of a human. This is a dynamic action where the elbow, wrist, and hand is used to release and spin a disk, allowing it to stably fly forwards (Fig. 1) [6]. Although a task at which humans can be extremely proficient, it is challenging to predict the optimal use of stiffness control for such a dynamical throwing motion. Whilst this a task that has been studied extensively from the perspective of sports science [7], skill learning and motivation [8], [9], biomechanics [10] and aerodynamics [11], there has been little experimental exploration of the role of stiffness and motor control of the arm when throwing. To study this behavior, we study how the passive dynamics of the joints of the arm affects the energy and motion of the disk.

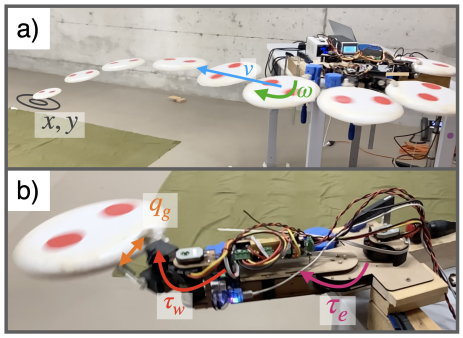

Fig. 1. a) Timelapse showing the Frisbee throw where the landing location, linear velocity and angular velocity is captured, b) The moment of release overlayed with the controllable parameters.

Although simulation approaches can be used, and have been in the past for a flying disk [12], high sensitivities in aerodynamic coefficients mean modelling errors are hard to eliminate. The addition of a robotic arm to release the disk in the system further complicates simulation based methods. We therefore choose and experimental approach for this study.

One significant challenging in realising a robotic Frisbee thrower is developing hardware where the joint stiffness can be controlled rapidly, precisely and programmatically, and over a large range of stiffness profiles while achieving the throwing motion [13]. Past works on dynamic walking and hopping robots has utilized series elastic actuators, where physical springs are used to store and release energy in the cyclical motion [14]. However, variation of stiffness requires swapping the springs, and in some cases further modification of the hardware. Instead of using springs, soft actuation can stiffness control through material properties [15], [16], but the range of stiffness and control bandwidth is often low and hence insufficient for more dynamics tasks. Variable stiffness (VS) actuators realizations through clever mechanisms have been proposed and fabricated [17], [18]. In particular for throwing tasks, [19] shows a single linked robot can throw a ball further thanks to the VS mechanism. [20] shows that the stiffness and motor position can be co-optimized to further improve the performance of ball throwing. However, a mechanical VS mechanism is complex to realise, design, and control. Another approach to achieve

[1]CREATE Lab, EPFL, Lausanne, Switzerland. Contact emails: kai.junge@epfl.ch, josie.hughes@epfl.ch.

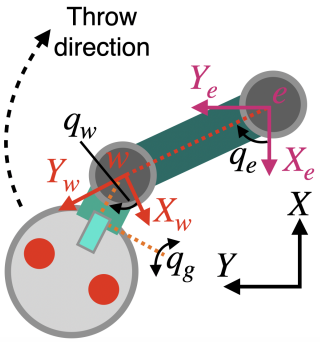

Fig. 2. Kinematic diagram of the experimental setup showing the coordinate systems used to define the motion.

VS is through impedance control. Dynamically throwing and catching objects with a robotic arm through impedance control is demonstrated in [21], [22]. This greatly reduces the mechanical design complexity, but in many cases specialized and expensive hardware to actuate a high reduction motor through closed loop with a force/torque sensor is necessary.

In this work, we leverage commercially available low-cost permanent magnet synchronous motors (PMSM) through a direct drive or "quasi-direct drive"(gear ratios lower than 1:10) configurations. This has several advantages such as efficient back-drivability and lower reflected inertia, and hence feed forward torque control can be performed, i.e.: by controlling the current input to the motor, the output torque can be accurately control without feedback from force/torque sensors. As its stiffness profile can be programmed, large numbers of experiments can be performed without hardware changes. Through this platform, the role of stiffness on the throwing behaviour (landing location and linear/angular velocity) is explored. Exploiting the programmable nature of the torque control, we also explore the contributions of varying the torque profile to other forms than simply placing a virtual stiffness. By comparing the wrist and elbow profiles of humans to that of a robot, we can gain some insights into the similarities of the two systems and the intricacies of the human motion compared to the robot.

The contribution of this work is two fold. First is the robotic arm using quasi-direct drive PMSMs to dynamically throw a Frisbee with the ability of controlling the stiffness. Second is the experimental investigation of Frisbee flight analysis and comparisons with a human.

II. Methods

A. Frisbee throwing robot setup

1) Robot configuration: The robotic setup comprises of a two-linked robot arm placed in parallel to the ground, mimicking the human elbow and wrist joint when throwing a Frisbee disk. The kinematic diagram of the robot is shown in Fig. 2, where the coordinate systems for each joint are described. The positions and velocities of the elbow and wrist are given by $q_e, \dot{q}_e$ and $q_w, \dot{q}_w$ respectively as shown in the figure. The gripper position q_g is controlled to be either in two states, open or closed. X, Y denotes the world coordinate system which is used to describe the behavior of the Frisbee throw.

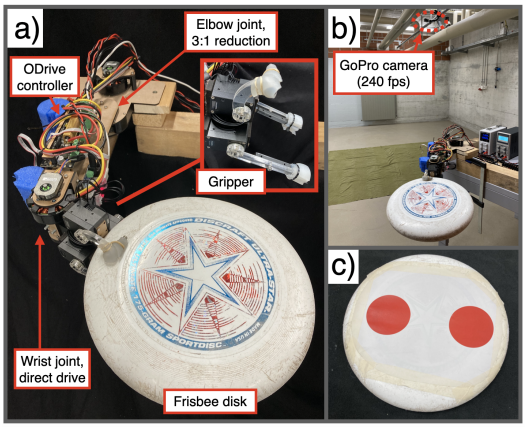

Fig. 3. a) The two joint elbow, wrist and hand setup with the held Frisbee. b) Experimental setup with overhead camera and c) Frisbee with visual markers to assist the computer vision assessment.

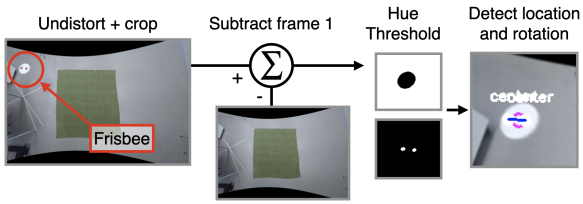

Fig. 4. Computer vision process to extract the Frisbee trajectory.

2) Experimental setup: Fig. 3a illustrates the robotic setup. At each joint, a PMSM (D5312S 330KV) from Odrive Robotics is used controlled by the ODrive v3.6 Board. Combined with encoders (AMT10E2-V), both motors can be controlled through field oriented control [23], allowing for precise and efficient motor control. While the wrist joint is a direct drive mechanism, the elbow joint is a quasi-direct drive with a 3:1 belt drive reduction to provide the necessary torque for the explosive motion without excessively increasing the reflected inertia. The gripper is comprised of three servo motors (Dynamixel XM430-W210-R), with acrylic fingers that have silicone rubber at its tips to firmly hold the disk.

All experiments are performed with the robotic setup mounted on a table horizontally at a height of 1m from the ground. The Frisbee disk is covered in white with two red circles (Fig. 3c), for its linear and angular positions to be read using computer vision.

3) Data collection and processing: A GoPro camera filming at 240fps is mounted on the ceiling to capture the flight trajectory (Fig. 3b). From the captured video, the approximate flight trajectory (approximate due to perspective effects of the camera) and the angular position of the disk is recorded. Fig. 4 illustrates this process. To obtain the landing location, the recorded sound from the GoPro camera used. The frame corresponding to the maximum sound amplitude, corresponds to the moment of landing.

B. Torque control and characterization

Throughout this work, to programatically change the stiffness, the wrist and elbow motors' torque (τ_e and τ_w as in Fig. 1b) must be controlled in relation to their angular position. By controlling the input current to the motor, the output

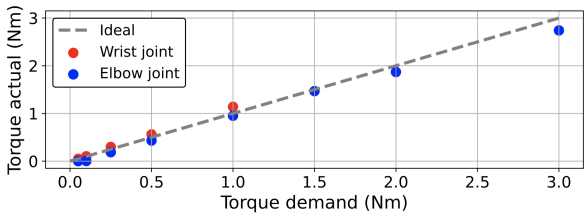

Fig. 5. Characterization of the static torque showing the demanded and measured torque for both the wrist and elbow joint.

torque can be controlled well without feedback control from force/torque sensors; for a motor with high back-drivability and low reflected inertia. The ODrive v3.6 control board is equipped with the ability to control the current input of the motor. Through a simple scaling, the current input can be translated to a demand torque in a feed-forward manner. To verify if the expected output torque of the motor is indeed the true output torque, a static and dynamic loading test is performed.

1) Static loading test: In the static loading test, each joint connected to a link is energized to statically load a 10kg Load cell, measuring the reaction force of the link to infer the static output torque. Fig. 5 shows the measured output torque of the wrist and elbow joint. It should be noted that the output torque of the elbow joint is *after* the 3:1 reduction. In both configurations the output torque is indeed close to the demand torque, which supports the use of this feed-forward current controller to control the output torque.

2) Dynamic testing: In conjunction with the the static test, the feed-forward output torque control is evaluated under dynamic conditions. A virtual spring-damper system was implemented as in Eq. 1 at a control frequency of $\approx$400Hz.

$$\begin{aligned} \tau_e &\approx \tau_{e,\text{Demand}} = -\left(k_e(q_e - q_e^{\text{eq}}) + d_e\dot{q}_e\right) \\ \tau_w &\approx \tau_{w,\text{Demand}} = -\left(k_w(q_w - q_w^{\text{eq}}) + d_w\dot{q}_w\right) \end{aligned} \tag{1}$$

$\tau_{i,\text{Demand}}$ is the feed-forward demand torque. The output torque is τ_i. k_i and d_i are stiffness and damping coefficients. q_i^{eq} is the equilibrium position of the spring. i should be replaced with e or w for the elbow and wrist respectively.

The first test performed is an impact test to qualitatively confirm if the behavior of the robot mimics a true spring. The top images in Fig. 6 shows the motion of the robot arm when hit by a hammer. Indeed, the motion mimicks the spring.

The second test is to compare the variation of the angular position of the virtual spring-damper loaded joint and an ideal simulated joint when given a step response in its equilibrium position. Here, q_w^{eq} was varied from 0 to $\pi/3$rad, $k_w = 0.5$, and $d_w = 0.01$. Two different inertia configurations were tested: low inertia (0.0008kgm^2) and high inertia (0.011kgm^2). Only the wrist axis is tested.

The bottom plot of Fig. 6 shows the variation of q_w against time for the two inertia conditions. Overlayed are the modelled responses of a mass-spring-damper system with the same inertia and stiffness values. The real and modelled trajectories match well, indicating the validity of the feed-forward torque control even for dynamic conditions. The only discrepancy is the damping, which is $d = 0.03$ in the model. This discrepancy is mostly likely due to damping

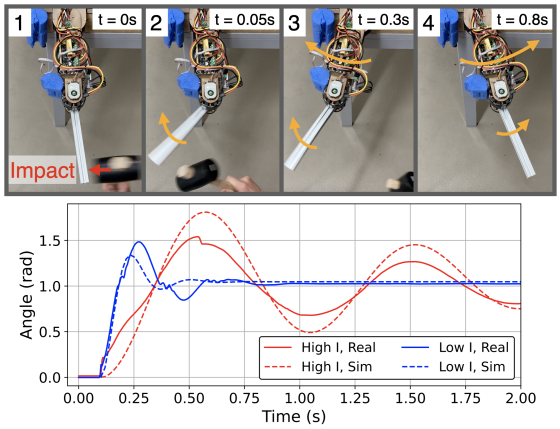

Fig. 6. Top: Pictorial results of an impact test to the wrist joint. Bottom: Wrist angular position of a step response for two different loading conditions for the measured and modelling response.

in the system which has been unaccounted for (damping in bearings, flexing of materials, etc).

Despite the minor damping discrepancy, the current controller is capable of controlling the output torque through feed-forward control in both static and dynamic cases.

C. Throw parameterization

The throw sequence is divided into three phases:

Phase 1: The motion is initialized from a starting position, q_w^{start}, q_e^{start}. It begins with the elbow actuated towards its end position q_e^{end} under a torque profile $T_e(q_e, \dot{q}_e)$ (subsequently defined). The wrist is equipped with a virtual spring with its equilibrium as the starting position $q_{w,\text{start}}$:

$$\begin{aligned} \tau_{w,\text{Demand}} &= -\left(k_{w,0}(q_w - q_w^{\text{start}}) + d_{w,0}\dot{q}_w\right) \\ \tau_{e,\text{Demand}} &= T_e(q_e, \dot{q}_e) \quad q_g = \text{CLOSE} \end{aligned} \tag{2}$$

Phase 2: When an elbow position $q_{e,\text{switch}}$ is reached, we transitions to phase 2. Here, the elbow is actuated identically to phase 1 (through $T_e(q_e, \dot{q}_e)$). Now the wrist is also actuated towards its end position q_e^{end} through $T_w(q_w, \dot{q}_w)$:

$$\begin{aligned} \tau_{w,\text{Demand}} &= T_w(q_w, \dot{q}_w) \\ \tau_{e,\text{Demand}} &= T_e(q_e, \dot{q}_e) \quad q_g = \text{CLOSE} \end{aligned} \tag{3}$$

Phase 3: When a particular wrist position $q_{w,\text{switch}}$ is reached, the gripper is commanded to open, to release the Frisbee:

$$\begin{aligned} \tau_{w,\text{Demand}} &= T_w(q_w, \dot{q}_w) \\ \tau_{e,\text{Demand}} &= T_e(q_e, \dot{q}_e) \quad q_g = \text{OPEN} \end{aligned} \tag{4}$$

The quantities $q_w^{\text{start}} = 40°$, $q_e^{\text{start}} = 10°$, $q_w^{\text{end}} = 135°$, $q_e^{\text{start}} = 130°$, $k_{w,0} = 2$, $d_{w,0} = 0.05$ are constant throughout the exploration. Using this throwing procedure, two actuation modes are explored, one with a fixed stiffness mimicking a physical spring, the other with variable stiffness. An example of a resulting throw trajectory is shown in Fig. 1a.

*1) **Mode 1**: Linear spring-damper (constant stiffness):* In this mode, we actuate the link as if real springs and dampers are in the joints. This is achieved by substituting the torque profile $T_e(\cdot)$ and $T_w(\cdot)$ with a spring-damper equation (5).

TABLE I

VALUES FOR THE THREE SETTINGS (A, B, C) USED FOR THE FOUR DIFFERENT PARAMETERS EXPLORED IN **MODE 1**.

Parameter	k_w	k_e	q_e^{switch}	q_w^{switch}
Setting A	0.05	0.6	85°	85°
Setting B	0.3	1.2	70°	70°
Setting C	1.8	2.4	55°	55°

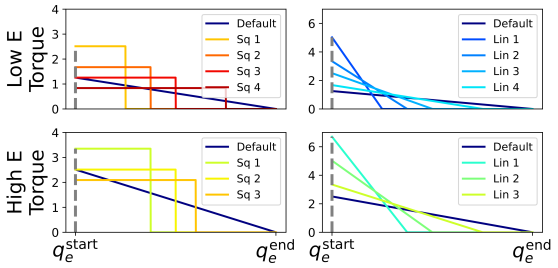

Fig. 7. Visualization of the torque profile in **mode 2** actuation.

$$T_w(q_w,\dot{q}_w) = -\left(k_w,(q_w - q_w^{\text{end}}) + d_w\dot{q}_w\right)$$
$$T_e(q_e,\dot{q}_e) = -\left(k_e,(q_e - q_e^{\text{end}}) + d_e\dot{q}_e\right) \quad (5)$$

Four parameters are explored with three settings (A, B, C) each as summarized in Table I: a total of 81 permutations. The damping is kept constant at $d_w = 0.005$ and $d_e = 0.01$.

*2) **Mode 2**: Variable elbow torque profile:* **Mode 2** is an extension of **mode 1**, but introduces variable torque profiles for the elbow actuation, i.e. $T_e(q_e,\dot{q}_e)$ is explored. In this mode, we evaluate the throwing distance with changes in elbow actuation (the wrist is omitted since the exploration of mode 1 highlights the elbow is the main contributor to distance. To clearly identify and explore how varying the torque profile affects the throw, other parameters introduced in **mode 1** are kept constant. To be able to meaningfully *compare* different torque profile, for each torque profile, the "energy" or $E = \int_{q_e^{\text{start}}}^{q_e^{\text{end}}} T_e(q_e,\dot{q}_e)\,dt$ is also kept constant. Two energy levels are considered, that of using the Setting A and B for k_e in **mode 1**; denoted at "Low E" and "High E".

Fig. 7 shows the $T_e(q_e,\dot{q}_e)$ to be tested. Square (constant torque) profiles (unachievable by simple springs) are compared to spring-like linear profiles. Compared to the baseline, all **mode 2** torque profiles reaches zero torque before the link is at the end position. We hypothesize, that a large initial torque provides the necessary acceleration for the maximum linear velocity at the release point.

D. Repeatability Test

The repeatability of the robot system is evaluated by testing three different settings in **mode 1** for five consecutive trials and evaluating the landing location. Fig. 8 shows the consistencies in the landing positions, and its low standard deviations in the distance r and angle θ from the point of release. Due to this reliability, every throw setting in the exploration will be performed once without repetition.

III. RESULTS

A. Constant stiffness throwing behavior

Fig. 9 illustrates the results from a full parameter sweep in **mode 1**, resulting in 81 throws. Through Fig. 9a-d, the

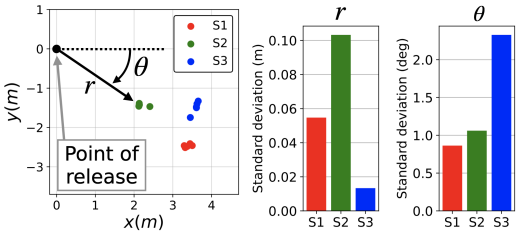

Fig. 8. Repeatability tests of the robotic system with five throws performed with 3 throw settings (S1, S2, S3). Landing positions and their standard deviation in distance and angle are shown.

variation of the parameters compared to the landing location is shown. A number of trends can be observed, firstly for a higher stiffness the throw distance r is longer. Secondly, with a delayed release timing, the throw angle θ is larger. There are however nuances, such as the effect of k_e on r is higher than that of k_w even through inspection. Fig. 9e,f shows how linear and angular velocity varies with the landing location. The trend in the variation of linear velocity is extremely clear, where the further throws have a larger v. The trend for ω is similar but there are some outliers. With a higher ω, the stability of the flight increases, increasing the throw. However, without a sufficient v, a disk with high ω doesn't travel far, which could explain the few outliers. The results agree with intuition of such a robotic throwing system.

Fig. 9g,h shows the distribution of v and ω for different stiffness settings. In Fig. 9g, a gradual increase in velocity is observed as the elbow stiffness setting k_e increases. Although less apparent, a similar trend can be seen for the wrist stiffness. On the other hand, ω is strongly coupled with k_w but weakly with k_e, showing the importance of the wrist "snap"[1] motion.

B. Constant energy variable torque profile throws

Fig. 10 shows the variation of the associated spring energy with the landing location, resulting in an extremely clear relationship between distance travelled and "energy levels". However, in **mode 1** the elbow continues to be actuated (supplied with energy). To investigate if the throwing distance can be improved with the same amount of energy while varying the torque profile, **mode 2** of the throwing motion is explored, and compared to the baseline torque profile, which is the **mode 1** actuation of the same energy level.

Fig. 11 shows the variation of landing position against the different settings in **mode 2**. The top plot shows the landing location for different torque profiles (as defined in Fig. 7). There is some variation in the landing position. In particular, throws with low energy vary much more in distance compared to that of the high energy, with explainable trends. For example, within the four square torque profiles, there is an *optimum* at the setting *Square 1*. As shown in Fig. 7, going from *Square 1* to *Square 4* the duration of which the torque is applied increase, while the applied torque value decreases (similarly for *Line 1* to *Line 4*). Hence, to maximise the throwing distance for a particular energy level,

[1] In Frisbee throwing, "snap" refers to a high acceleration motion of your wrist to increase the angular velocity of the disk.

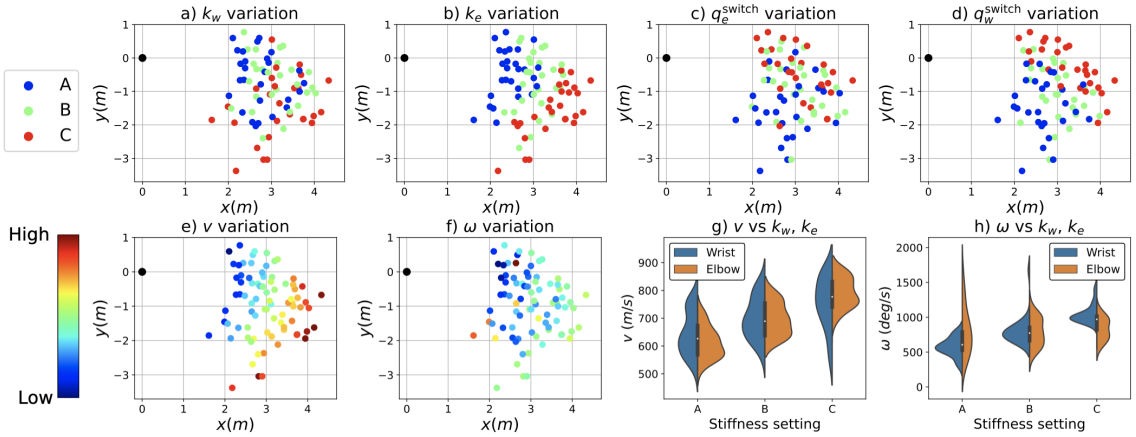

Fig. 9. Aggregate data of the systematic parameter exploration in **mode 1** actuation. a) - d) Variation in the four parameters vs the landing location. e), f) Variation of the linear and angular velocities (v, ω) vs the landing location. g), h) Distribution of throws with different values of v and ω under different settings of k_w and k_e.

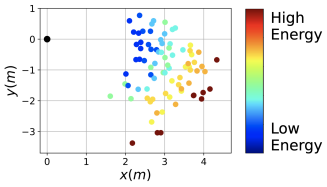

Fig. 10. Potential energy stored in wrist and elbow springs vs landing location.

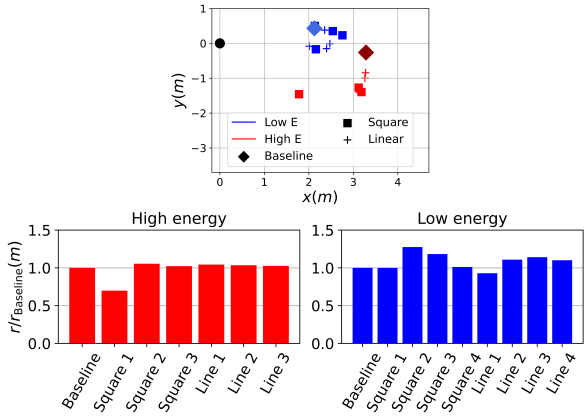

Fig. 11. Top: Landing location of disks thrown with settings in **mode 2** actuation. Bottom: Ratio of the distance from the origin r divided by the baseline distance r_{Baseline}, for the two energy levels.

the torque must be increased, but maintained until near the release moment. Equally, if the torque profile is sub-optimal, the throwing distance can be significantly worse, which is the case of *Square 1* at the higher energy level.

However, when considering the full region of where the robot can throw the disk and excluding outliers, the landing locations of each energy level is clustered. That is, the effect of varying the torque profile for a particular energy level is low compared to increasing the energy level it self. The maximum throwing distance r is dominated by the overall supply of energy, rather than how the energy is distributed.

C. Comparison of Human and Robot Frisbee Throwing

To compare human throws and robot throws, a target throwing competition was performed. In this experiment, a target box (approx 50cm x 50cm) was placed in two locations: *Short* at 3m and *Long* at 5m. For each target, both

TABLE II

SUCCESS RATE OF ALL THROWERS FOR THE TWO TARGETS.

Player:	Robot	Human 1	Human 2	Human 3
Short:	0.9	0.8	0.8	0.9
Long:	0.7	0.6	0.4	0.3

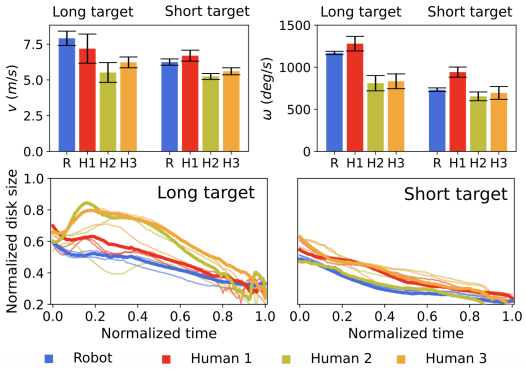

Fig. 12. Top: Mean v and ω for each player for both distance settings. Bottom: Variation of the size of the disk captured by the video over the flight time.

the robot and humans performed 10 consecutive throws. The robot's controller was chosen to be the setting from **mode 1** which is closest to the target.

Three humans throwers participated in the experiment. Human 1 is an *experienced* thrower whereas Humans 2 and 3 are *novice* throwers.

The success rate is shown in Table II for two targets. Success was determined to be landing the Frisbee fully inside the target. For the short target, the robot and all humans perform well with a success rate of over 80%. For the longer target, the robot outperformed all humans. A success rate of 70% was most comparable to an experienced human thrower, while novice throwers performed significantly worse.

Fig. 12 shows further comparisons between the human and robot. In the top plots, for both long and short targets, the robot's mean linear and angular velocities of the Frisbee were in similar ranges to all humans. The standard deviations were also comparable, but always consistently lower than humans, especially for the angular velocity. In most cases, the robot shows throwing behavior closest to the experienced thrower: human 1. Most clearly shown for the ω at the long target,

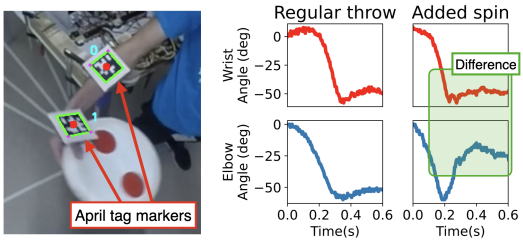

Fig. 13. Left: Capturing the human wrist and elbow motion using April Tag markers. Right: Variation of the wrist and elbow angular positions for two types of throws.

the robot and human 1 mark an angular speed roughly 1.5x larger than humans 2 and 3.

Similar observations are seen in the bottom plots of Fig. 12. Here, the variation of the disk size seen by the camera is plotted against its flight time. While perspective effects are present, a consistent flight trajectory results in a consistent variation of area over time. For the short target, all throwers' throws generate a reasonably consistent flight path, which led to consistent successes (Table II). Whereas, on the long target, the robot and human 1 produce consistent paths, while the variation of humans 2, 3 are higher across each throw.

From qualitative observation of the video recordings, humans 2 and 3 were "tossing" the disk almost with a parabolic path into the long target, while the robot and human 1 were throwing with higher speed and spin directly into the target, which correlates with the measurements.

1) Complex throwing motion in humans: While throw accuracy and consistency is important, the robotic setup and how the dynamics is controlled does not capture a large proportion of what humans are able to do at ease. For example, when prompted to "throw with a lot of spin", the human is able to intuitively modulate the dynamical motion of the elbow joint just in the moment of release, such that the friction of the fingers provide additional spin on the disk; while the wrist motion stays the same. The right hand plots in Fig. 13 show this difference in the human joint motion, in comparison to a "regular" throw.

IV. Discussion & Conclusion

Utilizing PMSM motors we develop an elbow and wrist structure of which we can control and investigate passive joint properties programmatically. We verify the simple feed-forward current control approach achieves good output torque control through the static and dynamic testing. Utilizing this programmable stiffness and modular robotic platform we explore different stiffness configurations for Frisbee throwing. The results are intuative and explainable, with the relationship between angular/linear velocity and landing location with respect to the throw parameters matching the physical understanding of the system. By exploring different torque profiles, we also demonstrate how the role of variable stiffness has a larger impact at lower energy levels.

By comparing to humans, the robot is able to perform most closely an experienced human thrower, outperforming in the accuracy of throws However, humans are able to exhibit a larger breadth of dynamical tasks. One such example is that presented in section III-C.1. Observations such as this, show the possibility of further exploration of this motion, even with a simple two-jointed robotic setup.

References

[1] S. Rapoport, J. Mizrahi, E. Kimmel, O. Verbitsky, and E. Isakov, "Constant and variable stiffness and damping of the leg joints in human hopping," *Journal of biomechanical engineering*, vol. 125, no. 4, pp. 507–514, 2003.

[2] D. J. Braun, M. Howard, and S. Vijayakumar, "Exploiting variable stiffness in explosive movement tasks," *Robotics: Science and Systems VII*, vol. 7, pp. 25–32, 2012.

[3] D. Braun, M. Howard, and S. Vijayakumar, "Optimal variable stiffness control: formulation and application to explosive movement tasks," *Autonomous Robots*, vol. 33, no. 3, pp. 237–253, 2012.

[4] H. Lipson, "Challenges and opportunities for design, simulation, and fabrication of soft robots," *Soft Robotics*, vol. 1, pp. 21–27, 2014.

[5] S. Wolf, T. Bahls, M. Chalon, W. Friedl, M. Grebenstein, H. Höppner, M. Kühne, D. Lakatos, N. Mansfeld, M. C. Özparpucu *et al.*, "Soft robotics with variable stiffness actuators: Tough robots for soft human robot interaction," in *Soft robotics*. Springer, 2015, pp. 231–254.

[6] V. Morrison, "The physics of frisbees," *Mount Allison University Physics Department*, vol. 1, 2005.

[7] E. Winograd and J. R. Engsberg, "Throwing techniques for ultimate frisbee," *The Sporf*, 2012.

[8] J.-F. Yang and J. Scholz, "Learning a throwing task is associated with differential changes in the use of motor abundance," *Experimental brain research*, vol. 163, no. 2, pp. 137–158, 2005.

[9] A. T. Latinjak, M. Masó, and N. Comoutos, "Goal-directed self-talk used during technical skill acquisition: The case of novice ultimate frisbee players," *The Sport Psychologist*, vol. 32, pp. 60–65, 2018.

[10] R. M. Bartlett, "The biomechanics of the discus throw: A review," *Journal of sports sciences*, vol. 10, no. 5, pp. 467–510, 1992.

[11] J. Potts and W. Crowther, "Frisbee (tm) aerodynamics," in *20th AIAA applied aerodynamics conference*, 2002, p. 3150.

[12] M. Hubbard and S. Hummel, "Simulation of frisbee flight," in *5th Conference on Mathematics and Computers in Sport*.

[13] S. Wolf, G. Grioli, O. Eiberger, W. Friedl, M. Grebenstein, H. Höppner, E. Burdet, D. G. Caldwell, R. Carloni, M. G. Catalano *et al.*, "Variable stiffness actuators: Review on design and components," *IEEE/ASME transactions on mechatronics*, vol. 21, no. 5, pp. 2418–2430, 2015.

[14] N. Paine, S. Oh, and L. Sentis, "Design and control considerations for high-performance series elastic actuators," *IEEE/ASME Transactions on Mechatronics*, vol. 19, no. 3, pp. 1080–1091, 2013.

[15] Y. Hao, T. Wang, and L. Wen, "A programmable mechanical freedom and variable stiffness soft actuator with low melting point alloy," in *International conference on intelligent robotics and applications*. Springer, 2017, pp. 151–161.

[16] F.-Y. Xu, F.-Y. Jiang, Q.-S. Jiang, and Y.-X. Lu, "Soft actuator model for a soft robot with variable stiffness by coupling pneumatic structure and jamming mechanism," *IEEE Access*, vol. 8.

[17] A. Bicchi, G. Tonietti, M. Bavaro, and M. Piccigallo, "Variable stiffness actuators for fast and safe motion control," in *Robotics research. The eleventh international symposium*.

[18] M. S. Lavate and R. Todkar, "Variable stiffness actuators: A general review," *International Journal of Engineering and Technical Research*, vol. 4, no. 7, pp. 201–205, 2015.

[19] S. Wolf and G. Hirzinger, "A new variable stiffness design: Matching requirements of the next robot generation," in *2008 IEEE International Conference on Robotics and Automation*, 2008, pp. 1741–1746.

[20] D. Braun, M. Howard, and S. Vijayakumar, "Optimal variable stiffness control: formulation and application to explosive movement tasks," *Autonomous Robots*, vol. 33, no. 3, pp. 237–253, Oct 2012. [Online]. Available: https://doi.org/10.1007/s10514-012-9302-3

[21] B. Bäuml, T. Wimböck, and G. Hirzinger, "Kinematically optimal catching a flying ball with a hand-arm-system," in *2010 IEEE/RSJ International Conference on Intelligent Robots and Systems*. IEEE, 2010, pp. 2592–2599.

[22] B. Bäuml, O. Birbach, T. Wimböck, U. Frese, A. Dietrich, and G. Hirzinger, "Catching flying balls with a mobile humanoid: System overview and design considerations," in *2011 11th IEEE-RAS International Conference on Humanoid Robots*, 2011, pp. 513–520.

[23] H. Le-Huy, "Comparison of field-oriented control and direct torque control for induction motor drives," in *Conference record of the 1999 IEEE industry applications conference. Thirty-forth IAS annual meeting (Cat. No. 99CH36370)*, vol. 2. IEEE, 1999, pp. 1245–1252.